

www.acsami.org Research Article

# Strain-Work Function Relationship in Single-Crystal Tetracene

Zhuoran Zhang, Guichuan Yu, Javier Garcia-Barriocanal, Zuoti Xie, and C. Daniel Frisbie\*



**Cite This:** ACS Appl. Mater. Interfaces 2020, 12, 40607–40612



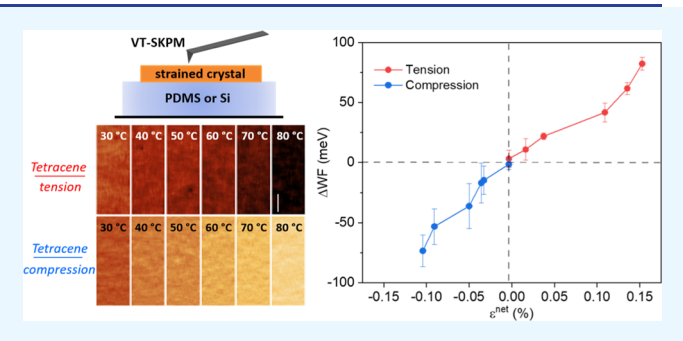
**ACCESS** 

Metrics & More



s Supporting Information

ABSTRACT: Understanding the impact of strain on organic semiconductors is important for the development of electronic devices and sensors that are subject to environmental changes and mechanical stimuli; it is also important for understanding the fundamental mechanisms of charge trapping. Following our previous study on the strain effects in rubrene, we present here only the second example of the strain—work function relationship in an organic semiconductor; in this case, the benchmark material tetracene. Thin, platelike single crystals of tetracene with large (001) facets were laminated onto silicon and rubber substrates having significantly different coefficients of thermal expansion;



mechanical strain in tetracene was subsequently induced by varying the temperature of the assembly. Tensile and compressive strains parallel to the (001) major facet were measured by grazing incidence X-ray diffraction, and the corresponding shifts in the electronic work functions were recorded via scanning Kelvin probe microscopy (SKPM). The work function of the tetracene (001) crystal surface directly correlated with the net mechanical strain and increased by  $\sim 100$  meV for in-plane tensile strains of 0.1% and decreased by approximately the same amount for in-plane compressive strains of -0.1%. This work provides evidence of the general and important impact of strain on the electrical properties of van der Waals bonded crystalline organic semiconductors and thereby supports the hypothesis that heterogeneous strains, for example in thin films, can be a major source of static electronic disorder.

KEYWORDS: single crystal, strain, work function, scanning Kelvin probe microscopy, X-ray diffraction, organic semiconductors

## **■ INTRODUCTION**

The envisioned applications of many organic electronic devices involve significant mechanical deformations associated with bending or stretching. Therefore, from the practical standpoint of developing flexible and stretchable electronics, it is important to understand the impact of strains on organic semiconductor electronic properties. More fundamentally, strains, and in particular inhomogeneous strains that arise during film deposition, are likely to be a significant source of electronic disorder in soft, van der Waals bonded organic semiconductors, and thus can lead to degraded electrical transport via charge carrier trapping and scattering.<sup>2-5</sup> For example, at a microscopic level, strains produce defects<sup>6</sup> such as dislocations, 7,8 stacking faults, 9 and subtle changes in intermolecular packing that modify both the local electronic site energies and the nonlocal overlap of adjacent molecular orbitals (highest occupied molecular orbital (HOMO) and lowest unoccupied molecular orbital (LUMO)). Within this framework, it is expected that strain-and in particular inhomogeneous strain—is capable of generating a spectrum of shallow and deep trap states 10 in the band gaps of organic semiconductors. Understanding the connection of strain to such electronic disorder is thus of fundamental importance for minimizing carrier trapping and improving organic semiconductor performance.

Unfortunately, there are very few studies to date that provide direct evidence of a connection between strain and static electronic disorder in organic semiconductors. This is in large part because of substantial experimental difficulties in resolving and correlating both strain and electronic properties on microscopic length scales.<sup>11</sup> Here, we directly address this issue by employing scanning Kelvin probe microscopy<sup>12–17</sup> (SKPM) to image organic semiconductor single crystals under different strain states. SKPM allows mapping of surface morphology and work function simultaneously, 18 and thus is one of the few experimental methods that can provide correlated structure and electrical information on ~100 nm length scales. 19-21 Single crystals, on the other hand, eliminate the substantial structural complexity typical of thin films<sup>22-</sup> and thus both enhance opportunities for quantitative analysis of strain  $(\varepsilon)$ -work function (WF) relationships, and relax spatial resolution requirements, as we demonstrate below.

Our study builds on our prior work describing the strain—work function relationship in single crystals of the well-known

Received: June 26, 2020 Accepted: August 10, 2020 Published: August 10, 2020





semiconductor rubrene.<sup>26</sup> In that work, we demonstrated a positive correlation between the strain state of rubrene and the work function of its (001) crystal face. We also noted that local variations in work function (e.g., across a crystalline thin film) reflect shifts in the vacuum level  $(E_{vac})$  and thus represent a direct measure of static electronic disorder: shifts in  $E_{\rm vac}$  also reflect HOMO and LUMO band edge shifts and lead to the formation of tail states in the band gap of organic semiconductors. In other words, we argued that measuring work function shifts as a function of strain constitutes a direct correlation of electronic disorder and strain. Since that study, related work on strain-induced defect formation, 27 energy-level alignment at metal/organic interfaces, 28 charge trapping, 5 and charge mobility enhancement, in the case of uniform compressive strain,<sup>29</sup> have been reported for single crystal and thin-film organic semiconductors. Yet, to the best of our knowledge, a quantitative strain-work function relationship has not been observed experimentally in organic semiconductors other than rubrene.

Here, we seek to expand our examination of strain  $(\varepsilon)$ —work function (WF) relationships to the case of single-crystal tetracene, which is a member of the well-known family of linear acene materials and which has also been studied extensively as an organic semiconductor. 30-35 Combining WF measurements on the (001) face with in-plane strain quantification under multiple strain conditions, we observe a correlation similar to rubrene, i.e., tensile strain leads to a substantial increase in WF, while compressive strain leads to a decrease in WF. Given the fact that tetracene 36,37 adopts a different crystal packing motif (triclinic P1) than rubrene<sup>38</sup> (orthorhombic *Cmca*), our new findings extend the generality of our previous investigation. Furthermore, our results provide quantitative support for the important hypothesis that inhomogeneous strains, so common in thin films, can be a principal source of electronic disorder (e.g., spatial band edge fluctuations) in organic thin-film devices.

# ■ RESULTS AND DISCUSSION

**Tetracene Single Crystals.** Tetracene powder source material was purchased from Sigma-Aldrich (98% purity). Single crystals of tetracene were grown using the physical vapor transport (PVT) method. The crystal adopts the triclinic  $P\overline{1}$  space group (Figure 1a,b), which contains two molecules in the unit cell and features a characteristic edge-to-face herringbone packing motif. The crystals used in the following strain experiments were thin platelets several millimeters in length and width and less than 1  $\mu$ m in thickness. The major facet of the crystal was the (001) plane, and the longest axis was aligned with the  $[1\overline{1}0]$  direction that was previously discovered to be the highest charge transport direction. The source of the crystal was the contained to the highest charge transport direction.

Tensile and Compressive Strains Induced via Crystal–Substrate Thermal Expansion Mismatch. The scheme for strain experiments is illustrated in Figure 1c,d. Freshly grown tetracene crystals were laminated onto poly-(dimethylsiloxane) (PDMS) or silicon (Si) substrates. The substrates were chosen due to their significantly different coefficients of thermal expansion (CTE,  $\alpha_{\rm PDMS} = 300 \times 10^{-6}$  K<sup>-1</sup>;  $\alpha_{\rm Si} = 3-4 \times 10^{-6}$  K<sup>-1</sup>) as compared to the tetracene crystal ( $\alpha_{\rm Tet} = 68 \times 10^{-6}$  K<sup>-1</sup> along [110]). Single-crystal tetracene with a thickness less than 1  $\mu$ m was adhered onto the substrates by simple lamination; adhesive was not necessary. As the single crystal was in contact with the substrate, upon

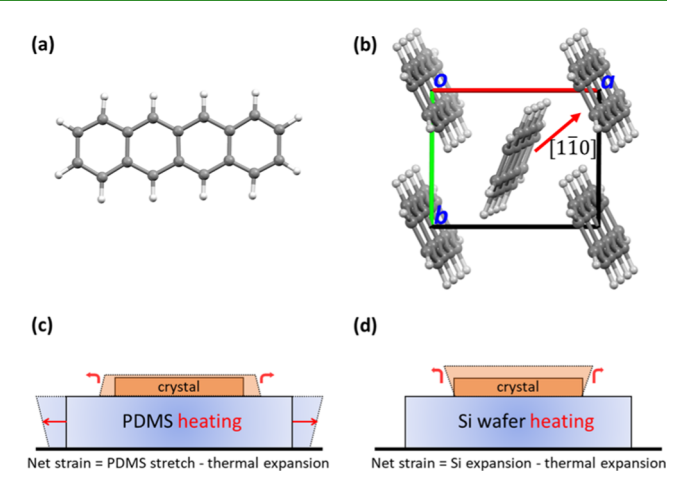


**Figure 1.** (a) Molecular structure of tetracene. (b) Tetracene packing motif in the a-b plane, the red arrow indicates the most efficient charge transport direction [110]. Unit cell parameters: a=7.90 Å, b=6.03 Å, c=13.53 Å,  $\alpha=100.3^{\circ}$ ,  $\beta=113.2^{\circ}$ , and  $\gamma=86.3^{\circ}$ . (c, d) Illustration of strain experiments. The red straight arrow indicates the thermal expansion of PDMS at the tetracene–PDMS interface. The red curved arrow indicates the thermal expansion of tetracene under strain. Dashed line-framed trapezoid indicates the final strained states of tetracene. The crystal experiences in-plane tensile strain in (c) and in-plane compressive strain in (d).

heating the sample above room temperature, mechanical strains were induced in the crystal due to thermal expansion mismatch between the crystal and the substrate. PDMS with a larger CTE than tetracene stretches the crystal in the in-plane direction more than the degree of its free thermal expansion. Since PDMS expands in an isotropic manner, anisotropic inplane net tensile strain is induced in tetracene. This net mechanical strain introduced to the crystal can be calculated by removing the thermal expansion component from the total strain  $\varepsilon^{\text{total}}$  measured by X-ray diffraction (XRD), that is,  $\varepsilon^{\text{net}}$  =  $arepsilon^{
m total} - arepsilon^{
m thermal}.$  In the out-of-plane direction, the free thermal expansion of tetracene crystal is suppressed by the Poisson effect due to the tensile stretch in the in-plane direction, and thus, a net compressive strain is introduced along the out-ofplane direction. In contrast, when silicon wafer is used as the substrate, the in-plane free thermal expansion of the single crystal is prohibited due to the much smaller CTE of silicon wafer, causing a net in-plane compressive strain. In the out-ofplane direction, a net tensile strain is introduced due to the Poisson effect and the in-plane constraints. In this study, we are particularly interested in the tensile/compressive strain induced within the (001) plane (the major facet) because this is the plane with substantial  $\pi$ - $\pi$  overlap and facile electrical transport.

Quantitative Strain Analysis by In Situ X-Ray Diffraction. To quantify the strain induced in tetracene crystals, temperature-dependent grazing incidence X-ray diffraction experiments were performed to monitor the change in tetracene interplanar spacings. By tracking the  $2\theta$  positions of the  $(1\overline{1}0)$  peak from 30 to 80 °C, the changes in d-spacings of tetracene  $d(1\overline{1}0)$  were calculated. Figure 2a shows the results of in-plane total strain along  $d(1\overline{1}0)$  induced in the single crystals using PDMS or Si substrates. At elevated temperature, the crystal experiences net expansion on both substrates, and the total strain along  $d(1\overline{1}0)$  was found to increase essentially linearly as temperature increases. However, the level of strain is significantly restricted on silicon wafer

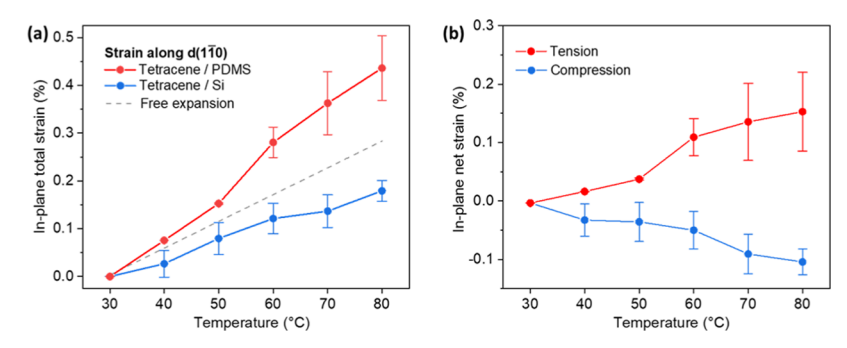
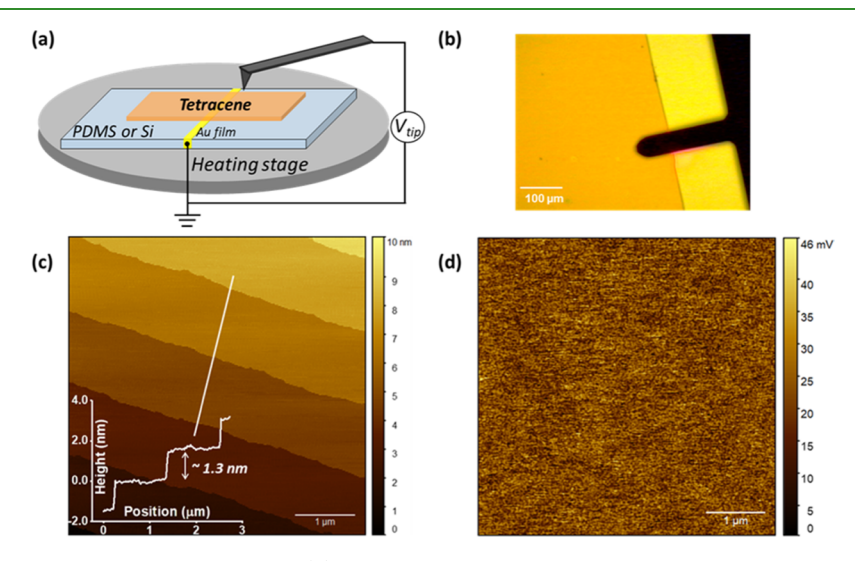


Figure 2. (a) Total  $d(1\overline{10})$  strain induced in tetracene crystals determined by temperature-dependent grazing incidence XRD measurements. Gray dashed line shows the free thermal expansion of tetracene based on experimentally determined CTE (see the Supporting Information). (b) Net  $d(1\overline{10})$  tensile and compressive strains induced in tetracene crystals.



**Figure 3.** (a) Schematic illustration of SKPM experiments. (b) Optical image of tetracene single crystal during an SKPM measurement. (c) Surface topography of tetracene single crystal shows a few flat terraces over a  $5 \times 5 \mu m^2$  area. The height difference between adjacent terraces corresponds to a single layer of tetracene molecules. Inset: height profile of the white line. (d) CPD image of tetracene showing uniform surface potential.

compared to PDMS. At 80 °C, the total strain along  $d(1\overline{10})$  induced on tetracene reached  $\varepsilon^{\text{total}} = 0.44\%$  ( $\pm 0.07\%$ ) on PDMS and only 0.18% ( $\pm 0.02\%$ ) on silicon wafer. Upon subtracting the free thermal expansion of  $d(1\overline{10})$  (calculated from unit cell measurements of free-standing tetracene crystals, see Table S1) from the total strain, the net mechanical strain along  $d(1\overline{10})$  was quantified. As shown in Figure 2b, PDMS-supported tetracene crystals experienced net mechanical tensile strains up to  $\varepsilon^{\text{net}} = +0.16\%$  ( $\pm 0.07\%$ ), while crystals on silicon wafer substrates exhibited net compressive strains up to  $\varepsilon^{\text{net}} = -0.09\%$  ( $\pm 0.02\%$ ).

Work Function Measurements by Temperature-Dependent SKPM. Upon quantifying the strain states as a function of temperature, we then utilized temperature-dependent SKPM to measure the change in the WF of tetracene (001) over the same temperature increments. The instrument setup for SKPM measurements is illustrated in Figure 3a,b, which operates in a two-pass "lift-mode" capable of mapping the topographic and electronic features simultaneously. According to the working mechanism of SKPM,  $^{15,18}$  the measured electronic signal is the contact potential difference (CPD) between the atomic force microscopy (AFM) probe and the surface of tetracene crystal, defined as CPD =  $(WF_{probe} - WF_{sample})/q$ , where q is the elementary charge. The conductive probes used in this paper were coated with Pt–Ir, whose work function has a weak temperature

dependence<sup>40</sup> (<10 mV change between the temperature extremes used in this paper). Given the fact that the individual work functions of AFM probes can vary, the same probe must be used throughout the measurements for a given sample. With WF<sub>probe</sub> acting as a reference, the WF change in the single crystal can be obtained from the CPD changes measured at different temperatures, i.e.,  $q\Delta CPD = -(WF_{sample}^{T2} - WF_{sample}^{T1})$  $= -\Delta WF$ . Figure 3c,d shows typical topography and surface potential data collected by scanning across a  $5 \times 5 \mu \text{m}^2$  area at room temperature. The surface height image shows a flat crystal domain containing a few crystal step edges. The height of each step is measured to be  $\sim$ 1.4 nm, which matches the lattice spacing of the tetracene (001) plane (13.5 Å). This also confirms that the major facet of the crystal is the (001) plane. Note that despite the existence of step edges, the SKPM image shows a featureless, uniform surface potential. The root-meansquare (RMS) roughness for the surface potential map is 5.6 mV for the scanned area. These results reflect the highly ordered molecular packing of tetracene single crystals and the electronic homogeneity of the tetracene (001) plane. This observation is consistent with previous SKPM measurements of pristine rubrene.<sup>26</sup>

Figure 4a shows the change in CPD for tetracene as a function of temperature on PDMS and silicon substrates. For PDMS-supported tetracene, as the temperature increased from 30 to 80  $^{\circ}$ C, the measured CPD dropped by  $\sim$ 80 ( $\pm$ 5) mV as

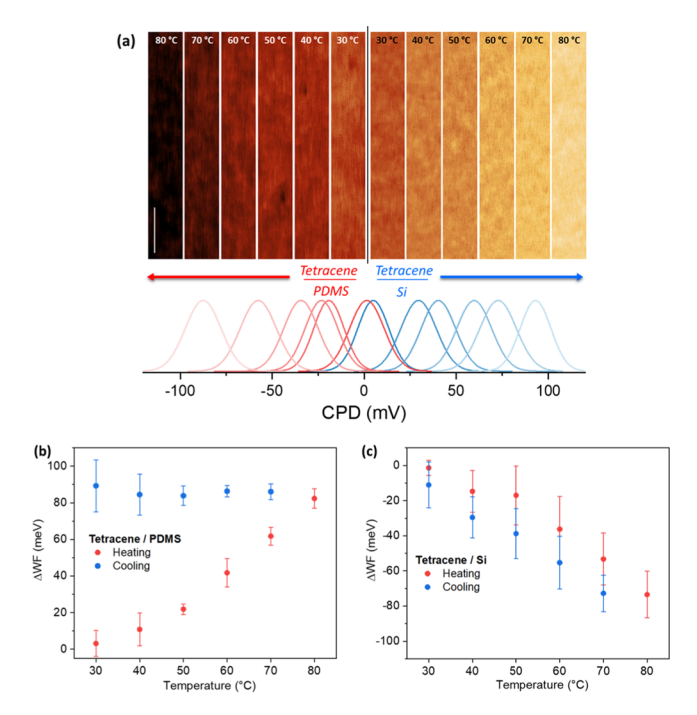


Figure 4. Temperature-dependent SKPM measurements of tetracene single crystals. (a) Change in CPD as a function of temperature on PDMS and silicon. On PDMS, the color of the CPD map changed from midpoint color to dark with the histogram (red) shifting to negative CPD; on silicon, the color of the CPD map changed from midpoint to bright with the histogram (blue) shifting to positive CPD. Length of the scale bar, 1  $\mu$ m. Averaged  $\Delta$ WF of tetracene on PDMS (b) and silicon (c) as a function of temperature.

indicated by the series of progressively darkened CPD maps. In contrast, for tetracene on silicon wafer, the CPD increased about 80 ( $\pm 13$ ) mV when heated to 80 °C, as shown in a series of progressively lightened CPD maps. By averaging the SKPM measurements on multiple samples, the change in WF ( $\Delta$ WF =  $-q\Delta$ CPD) was plotted as a function of temperature (Figure 4b,c). Upon heating, tetracene on PDMS showed a positive linear relationship between WF and temperature. Tetracene on silicon wafer, on the other hand, showed a negative linear decrease in WF. Interestingly, when comparing the data measured during cooling, distinctly different behaviors were found for the two substrates. On PDMS, the tetracene WF exhibited almost no response to temperature drop and a permanent WF shift of approximately 90 ( $\pm 14$ ) meV remained after cooling to 30 °C. However, on silicon wafer, the tetracene

WF recovered upon cooling with little hysteresis. Overall, the WF behavior in response to temperature is substantially different on PDMS and silicon wafer substrates. We attribute the difference in reversibility to the type of mechanical strain induced in the crystal, which will be discussed in the Correlation Between Strain and Work Function section.

Correlation Between Strain and Work Function. With both strain along  $d(1\overline{1}0)$  and the (001) WF measured as a function of temperature, we then plotted  $\Delta WF$  against total  $d(1\overline{10})$  strain and net  $d(1\overline{10})$  strain (Figure 5). Comparing the sign of WF changes in Figure 5a, we note that although tetracene experienced net expansion along  $d(1\overline{1}0)$  when heated on both substrates, the WF trends are completely opposite. This fact rules out both temperature and total strain as dominant factors responsible for  $\Delta$ WF. However, as discussed above, the substrate type does lead to either net tensile or compressive strain in the crystal upon increasing temperature. Therefore, it is reasonable to examine  $\Delta WF$ versus  $\varepsilon^{\rm net}$ . As shown in Figure 5b,  $\Delta$ WF increased significantly and monotonically with tension and decreased in a similar manner with compression. At 0.16% net tension, the WF of tetracene increased by ~80 meV, which is more than 3 times of  $k_{\rm B}T$  (25 meV) at room temperature. In contrast, with 0.09% net compression, the WF decreased by 80 meV. We believe that it is not coincidental that these changes in WF are comparable to the energies of shallow traps in many organic semiconductor thin films that lie in the range of 0–100 meV.<sup>3,4</sup>

Our results demonstrate that, in a manner similar to rubrene, the change in WF for tetracene is correlated with the magnitude and sign of net strain. Considering  $\Delta WF$  for crystals under tension, we observe that the  $\Delta WF-\varepsilon^{\rm net}$  relationship is approximately linear. Unlike our previous results on rubrene,  $^{26}$  we did not notice a sharp slope change for the  $\Delta WF-\varepsilon^{\rm net}$  curve that we previously suggested was an indication of the occurrence of an elastic-to-plastic transition (i.e., a yield point). However, given the large hysteresis in Figure 4b and comparing the heating—cooling traces for  $\varepsilon^{\rm total}-T$  on PDMS and silicon (Figures S4 and S5), it is reasonable to believe that the tetracene yield point is reached within the range of tensile strain achieved on the PDMS substrate.

# **■** CONCLUSIONS

In summary, we have demonstrated a correlation between mechanical strain and electronic work function in single-crystal tetracene. Utilizing thermal expansion mismatch between single crystals and corresponding substrates, net tensile and compressive strains were induced in the crystals. By performing

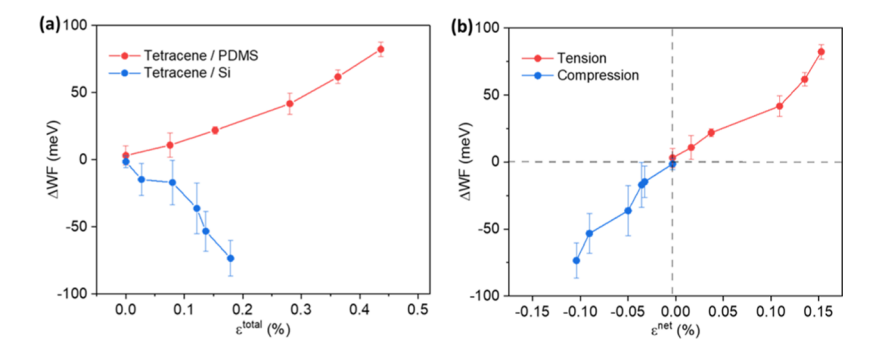


Figure 5. (a)  $\Delta$ WF as a function of  $\varepsilon$ <sup>total</sup> along  $d(1\overline{1}0)$  direction for tetracene on PDMS (red) and silicon (blue). (b)  $\Delta$ WF as a function of  $\varepsilon$ <sup>net</sup> along  $d(1\overline{1}0)$  direction for tetracene under tensile (red) and compressive (blue) strain.

temperature-dependent X-ray diffraction and SKPM experiments, mechanical strain and electronic work function were quantitatively correlated. Under tension, the work function of the tetracene (001) crystal face was found to increase as net tensile strain increased. The resulting change in WF was irreversible as net tension reached 0.16%. Under compression, the opposite trend was found, i.e., work function decreased with increasing compressive strain, and was reversible up to  $\varepsilon^{\rm net}$  = -0.09%. Our findings for tetracene provide further evidence of a definitive strain–WF correlation in organic semiconductors. Collectively, this work, together with our previous work on rubrene, also strongly suggests that strain, particularly inhomogeneous strain typical of thin films, can be a source of electronic disorder in crystalline organic semiconductors.

#### ASSOCIATED CONTENT

### Supporting Information

The Supporting Information is available free of charge at https://pubs.acs.org/doi/10.1021/acsami.0c11566.

Experimental details for sample preparation methods; temperature-dependent XRD and SKPM experiments; and tabulated experimental data (PDF)

#### AUTHOR INFORMATION

#### **Corresponding Author**

C. Daniel Frisbie — Department of Chemical Engineering and Materials Science, University of Minnesota, Minneapolis, Minnesota 55455, United States; Occid.org/0000-0002-4735-2228; Email: frisbie@umn.edu

#### Authors

**Zhuoran Zhang** — Department of Chemical Engineering and Materials Science, University of Minnesota, Minneapolis, Minnesota 55455, United States; orcid.org/0000-0002-3715-2740

**Guichuan Yu** – Characterization Facility and Informatics Institute, University of Minnesota, Minneapolis, Minnesota 55455, United States

Javier Garcia-Barriocanal – Characterization Facility, University of Minnesota, Minneapolis, Minnesota 55455, United States

Zuoti Xie — Department of Chemical Engineering and Materials Science, University of Minnesota, Minneapolis, Minnesota 55455, United States; Ocid.org/0000-0002-1828-0122

Complete contact information is available at: https://pubs.acs.org/10.1021/acsami.0c11566

#### Notes

The authors declare no competing financial interest.

#### ACKNOWLEDGMENTS

This work was primarily supported by the National Science Foundation under Grant no. DMR-1806419. Part of this work was carried out in the Characterization Facility, University of Minnesota, which received partial support from NSF through the MRSEC program under Grant no. DMR-1420013.

#### REFERENCES

(1) Coropceanu, V.; Cornil, J.; da Silva Filho, D. A.; Olivier, Y.; Silbey, R.; Brédas, J.-L. Charge Transport in Organic Semiconductors. *Chem. Rev.* **2007**, *107*, 926–952.

- (2) Kang, J. H.; da Silva Filho, D. A.; Bredas, J. L.; Zhu, Z.-Y. Shallow trap states in pentacene thin films from molecular sliding. *Appl. Phys. Lett.* **2005**, *86*, No. 152115.
- (3) Kalb, W. L.; Meier, F.; Mattenberger, K.; Batlogg, B. Defect healing at room temperature in pentacene thin films and improved transistor performance. *Phys. Rev. B* **2007**, *76*, No. 184112.
- (4) Kalb, W. L.; Haas, S.; Krellner, C.; Mathis, T.; Batlogg, B. Trap Density of States in Small-Molecule Organic Semiconductors: A Quantitative Comparison of Thin-Film Transistors with Single Crystals. *Phys. Rev. B* **2010**, *81*, No. 155315.
- (5) Mei, Y.; Diemer, P. J.; Niazi, M. R.; Hallani, R. K.; Jarolimek, K.; Day, C. S.; Risko, C.; Anthony, J. E.; Amassian, A.; Jurchescu, O. D. Crossover from band-like to thermally activated charge transport in organic transistors due to strain-induced traps. *Proc. Natl. Acad. Sci. U.S.A.* 2017, 114, E6739–E6748.
- (6) Alkauskas, A.; McCluskey, M. D.; Van de Walle, C. G. Tutorial: Defects in semiconductors Combining experiment and theory. *J. Appl. Phys.* **2016**, *119*, No. 181101.
- (7) Olson, I. A.; Shtukenberg, A. G.; Kahr, B.; Ward, M. D. Dislocations in molecular crystals. *Rep. Prog. Phys.* **2008**, *81*, No. 096501.
- (8) Andre, C. L.; Wilt, D. M.; Pitera, A. J.; Lee, M. L.; Fitzgerald, E. A.; Ringel, S. A. Impact of dislocation densities on n<sup>+</sup>/p and p<sup>+</sup>/n junction GaAs diodes and solar cells on SiGe virtual substrates. *J. Appl. Phys.* **2005**, *98*, No. 014502.
- (9) Wu, Y.; Ren, X.; McGarry, K. A.; Bruzek, M. J.; Douglas, C. J.; Frisbie, C. D. Scanning Kelvin Probe Microscopy Reveals Planar Defects Are Sources of Electronic Disorder in Organic Semiconductor Crystals. *Adv. Electron. Mater.* **2017**, *3*, No. 1700117.
- (10) Haneef, H. F.; Zeidell, A. M.; Jurchescu, O. D. Charge carrier traps in organic semiconductors: a review on the underlying physics and impact on electronic devices. *J. Mater. Chem. C* **2020**, *8*, 759–787.
- (11) Simoen, E.; Lauwaert, J.; Vrielinck, H. Analytical Techniques for Electrically Active Defect Detection. In *Semiconductors and Semimetals*; Romano, L.; Privitera, V.; Jagadish, C., Eds.; Elsevier, 2015; Vol. 91, pp 205–250.
- (12) Nonnenmacher, M.; O'Boyle, M. P.; Wickramasinghe, H. K. Kelvin probe force microscopy. *Appl. Phys. Lett.* **1991**, *58*, 2921–2923.
- (13) Fujihira, M. Kelvin Probe Force Microscopy of Molecular Surfaces. *Annu. Rev. Mater. Sci.* **1999**, 29, 353–380.
- (14) Glatzel, T.; Sadewasser, S.; Shikler, R.; Rosenwaks, Y.; Lux-Steiner, M. C. Kelvin probe force microscopy on III-V semi-conductors: The effect of surface defects on the local work function. *Mater. Sci. Eng., B* **2003**, *102*, 138–142.
- (15) Shen, Y.; Barnett, D. M.; Pinsky, P. M. Simulating and interpreting Kelvin probe force microscopy images on dielectrics with boundary integral equations. *Rev. Sci. Instrum.* **2008**, *79*, No. 023711.
- (16) Melitz, W.; Shen, J.; Kummel, A. C.; Lee, S. Kelvin probe force microscopy and its application. *Surf. Sci. Rep.* **2011**, *66*, 1–27.
- (17) Lee, H.; Lee, W.; Lee, J. H.; Yoon, D. S. Surface potential analysis of nanoscale biomaterials and devices using Kelvin probe force microscopy. *J. Nanomater.* **2016**, 2016, No. 4209130.
- (18) Xu, J.; Wu, Y.; Li, W.; Xu, J. Surface potential modeling and reconstruction in Kelvin probe force microscopy. *Nanotechnology* **2017**, 28, No. 365705.
- (19) Ellison, D. J.; Lee, B.; Podzorov, V.; Frisbie, C. D. Surface Potential Mapping of SAM-Functionalized Organic Semiconductors by Kelvin Probe Force Microscopy. *Adv. Mater.* **2011**, 23, 502–507.
- (20) He, T.; Wu, Y.; D'Avino, G.; Schmidt, E.; Stolte, M.; Cornil, J.; Beljonne, D.; Ruden, P. P.; Würthner, F.; Frisbie, C. D. Crystal step edges can trap electrons on the surfaces of n-type organic semiconductors. *Nat. Commun.* **2018**, *9*, No. 2141.
- (21) Salerno, M.; Dante, S. Scanning Kelvin Probe Microscopy: Challenges and Perspectives towards Increased Application on Biomaterials and Biological Samples. *Materials* **2018**, *11*, No. 951.

- (22) de Boer, R. W. I.; Gershenson, M. E.; Morpurgo, A. D.; Podzorov, A. Organic single-crystal field-effect transistors. *Phys. Status Solidi A* **2004**, 201, 1302–1331.
- (23) Liu, C.; Minari, T.; Lu, X.; Kumatani, A.; Takimiya, K.; Tsukagoshi, K. Solution-Processable Organic Single Crystals with Bandlike Transport in Field-Effect Transistors. *Adv. Mater.* **2011**, 23, 523–526.
- (24) Minder, N. A.; Lu, S.; Fratini, S.; Ciuchi, S.; Facchetti, A.; Morpurgo, A. F. Tailoring the molecular structure to suppress extrinsic disorder in organic transistors. *Adv. Mater.* **2014**, *26*, 1254–1260
- (25) McGarry, K. A.; Xie, W.; Sutton, C.; Risko, C.; Wu, Y.; Young, V. G.; Bredas, J. L.; Frisbie, C. D.; Douglas, C. J. Rubrene-based single-crystal organic semiconductors: Synthesis, electronic structure, and charge-transport properties. *Chem. Mater.* **2013**, 25, 2254–2263.
- (26) Wu, Y.; Chew, A. R.; Rojas, G. A.; Sini, G.; Haugstad, G.; Belianinov, A.; Kalinin, S. V.; Li, H.; Risko, C.; Brédas, J.-L.; Salleo, A.; Frisbie, C. D. Strain effects on the work function of an organic semiconductor. *Nat. Commun.* **2016**, *7*, No. 10270.
- (27) Cramer, T.; Travaglini, L.; Lai, S.; Patruno, L.; de Miranda, S.; Bonfiglio, A.; Cosseddu, P.; Fraboni, B. Direct imaging of defect formation in strained organic flexible electronics by Scanning Kelvin Probe Microscopy. *Sci. Rep.* **2016**, *6*, No. 38203.
- (28) Atxabal, A.; McMillan, S. R.; García-Arruabarrena, B.; Parui, S.; Llopis, R.; Casanova, F.; Flatté, M. E.; Hueso, L. E. Strain Effects on the Energy-Level Alignment at Metal/Organic Semiconductor Interfaces. ACS Appl. Mater. Interfaces 2019, 11, 12717–12722.
- (29) Choi, H. H.; Yi, H. T.; Tsurumi, J.; Kim, J. J.; Briseno, A. L.; Watanabe, S.; Takeya, J.; Cho, K.; Podzorov, V. A Large Anisotropic Enhancement of the Charge Carrier Mobility of Flexible Organic Transistors with Strain: A Hall Effect and Raman Study. *Adv. Sci.* **2020**, *7*, No. 1901824.
- (30) de Boer, R. W. I.; Klapwijk, T. M.; Morpurgo, A. F. Field-effect transistors on tetracene single crystals. *Appl. Phys. Lett.* **2003**, *83*, 4345.
- (31) Newman, C. R.; Chesterfield, R. J.; Merlo, J. A.; Frisbie, C. D. Transport properties of single-crystal tetracene field-effect transistors with silicon dioxide gate dielectric. *Appl. Phys. Lett.* **2004**, *85*, 422.
- (32) Anthony, J. E. The Larger Acenes: Versatile Organic Semiconductors. *Angew. Chem., Int. Ed.* **2008**, 47, 452–483.
- (33) Wang, C.; Dong, H.; Jiang, L.; Hu, W. Organic semiconductor crystals. *Chem. Soc. Rev.* **2018**, 47, 422–500.
- (34) Xia, Y.; Kalihari, V.; Frisbie, C. D.; Oh, N. K.; Rogers, J. A. Tetracene air-gap single-crystal field-effect transistors. *Appl. Phys. Lett.* **2007**, *90*, No. 162106.
- (35) Ostroverkhova, O.; Cooke, D. G.; Hegmann, F. A.; Anthony, J. E.; Podzorov, V.; Gershenson, M. E.; Jurchescu, O. D.; Palstra, T. T. M. Ultrafast carrier dynamics in pentacene, functionalized pentacene, tetracene, and rubrene single crystals. *Appl. Phys. Lett.* **2006**, 88, No. 162101
- (36) Robertson, J. M.; Sinclair, V. C.; Trotter, J. The Crystal and Molecular Structure of Tetracene. *Acta Crystallogr.* **1961**, *14*, 697–704.
- (37) Campbell, R. B.; Robertson, J. M.; Trotter, J. The crystal structure of hexacene, and a revision of the crystallographic data for tetracene and pentacene. *Acta Crystallogr.* **1962**, *15*, 289–290.
- (38) Henn, D. E.; Williams, W. G.; Gibbons, D. J. Crystallographic data for an orthorhombic form of rubrene. *J. Appl. Crystallogr.* **1971**, *4*, 256.
- (39) Laudise, R. A.; Kloc, C.; Simpkins, P. G.; Siegrist, T. Physical vapor growth of organic semiconductors. *J. Cryst. Growth* **1998**, *187*, 449–454.
- (40) Ibragimov, K. I.; Korol'kov, V. A. Temperature dependence of the work function of metals and binary alloys. *Inorg. Mater.* **2001**, *37*, 567–572.